

# Measuring the role of surface chemistry in silicon microphotronics

Matthew Borselli,\* Thomas J. Johnson, and Oskar Painter

*Department of Applied Physics, California Institute of Technology, Pasadena, CA 91125, USA.*<sup>†</sup>

(Dated: November 26, 2024)

PACS numbers:

The silicon/silicon dioxide (Si/SiO<sub>2</sub>) interface plays a crucial role in the performance, cost, and reliability of most modern microelectronic devices[1, 2, 3, 4, 5, 6, 7, 8], from the basic transistor to flash memory, digital cameras, and solar cells. Today the gate oxide thickness of modern transistors is roughly 5 atomic layers, with 8 metal wire layers required to transport all the signals within a microprocessor. In addition to the increasing latency of such reduced-dimension metal wires, further “Moore’s Law” scaling of transistor cost and density is predicted to saturate in the next decade[9]. As a result, silicon-based microphotronics is being explored for the routing and generation of high-bandwidth signals[10, 11, 12, 13, 14, 15, 16]. In comparison to the extensive knowledge of the electronic properties of the Si/SiO<sub>2</sub> interface, little is known about the optical properties of Si surfaces used in microphotronics. In this Letter, we explore the optical properties of the Si surface in the telecommunication-relevant wavelength band of  $\lambda = 1400\text{-}1600$  nm. Utilizing a high quality factor ( $Q \sim 1.5 \times 10^6$ ) optical microresonator[17] to provide sensitivity down to a fractional surface optical loss of  $\alpha'_s \sim 10^{-7}$ , we show that optical loss within Si microphotonic components can be dramatically altered by Si surface preparation, with  $\alpha'_s \sim 2 \times 10^{-5}$  measured for chemical oxide surfaces as compared to  $\alpha'_s \leq 2 \times 10^{-6}$  for hydrogen-terminated Si surfaces. These results indicate that the optical properties of Si surfaces can be significantly and reversibly altered by standard microelectronics treatments, and that stable, high optical quality surface passivation layers will be critical in future Si micro- and nano-photonic systems.

Historically, studies of Si surface and interface states have primarily focused on their electronic properties, with sensitive techniques such as deep-level transient spectroscopy[18] or surface-sensitive minority carrier lifetime measurements[6] being employed. Three exceptions to this are deep-level optical spectroscopy[19], cavity-ringdown spectroscopy[20], and the ultra-sensitive technique of photothermal deflection spectroscopy (PDS)[21, 22] which can measure fractional optical absorption down to  $\alpha l \sim 10^{-8}$ . None of the aforementioned techniques, however, is well suited for studying as-processed mi-

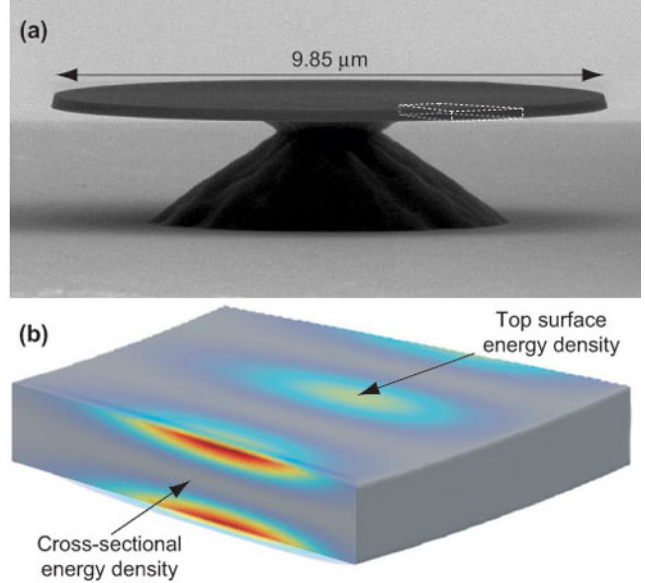


FIG. 1: Composite of surface-sensitive thin-disk optical resonance. (a) SEM micrograph of a  $5 \mu\text{m}$  radius SOI microdisk. (b) Zoomed-in representation of disk edge (white dashed box) showing a TM polarized whispering gallery mode solved via FEM, indicating large electric field energy density at the top and bottom surface of the silicon active layer.

crophotonic elements. In this work we utilize a specially designed microdisk optical resonator to study the optical properties of surfaces typical in silicon-on-insulator (SOI) microphotonic elements in a noninvasive, rapid, and sensitive manner. Shown in Figure 1, the high quality factor ( $Q$ ) Si microdisk resonators used in this work provide surface-specific optical sensitivity due to the strong overlap of the top and bottom surfaces of the active Si layer with the electric field energy density of appropriately polarized bound optical modes of the microdisk. In addition, light within these micron-scale structures circulates tens of thousands of times, providing an effective path length approaching one meter.

A normalized measure of surface sensitivity for a guided-wave mode in a waveguide or resonator can be defined as  $\Gamma'_s \equiv \Gamma_s/t_s$ , where  $\Gamma_s$  is the fractional electric field energy overlap with a surface perturbation of physical depth  $t_s$ . If optical loss is dominated by interactions with the surface, then the modal loss coefficient per unit length ( $\alpha_m$ ) measured from experiment can be related to a fractional loss per pass through the surface given by  $\alpha'_s = \alpha_m/\Gamma'_s$ . As discussed in Ref. [23], for a true two-

\*Electronic address: borselli@caltech.edu

<sup>†</sup>URL: <http://copilot.caltech.edu>

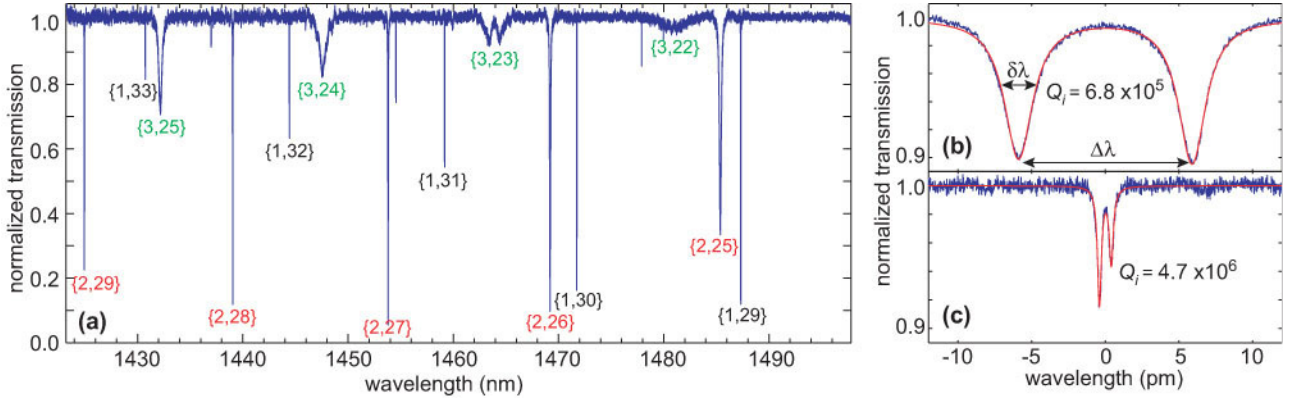


FIG. 2: Normalized spectral transmission response of Si microdisk resonators. (a) Broad scan across  $\lambda = 1400$  nm band for a  $5 \mu\text{m}$  radius microdisk with the fiber taper placed  $0.6 \pm 0.1 \mu\text{m}$  away from the disk edge and optimized for TM coupling. The spectrum was normalized to the response of the fiber taper moved  $3 \mu\text{m}$  laterally away from the disk edge. Each mode is labelled as  $\{p, m\}$  where  $p$  and  $m$  are the radial and azimuthal number, respectively. (b) High-resolution scan of the  $\text{TM}_{1,31}$  mode at  $\lambda = 1459$  nm in (a).  $\Delta\lambda$  and  $\delta\lambda$  indicate the CW/CCW mode splitting and individual mode linewidth, respectively. (c) High-resolution scan of a  $40 \mu\text{m}$  radius microdisk, showing the reduced loss of a bulk TE WGM.

dimensional surface in which the perturbation depth is infinitesimal,  $\alpha'_s$  is the most relevant quantity describing the surface and is equivalent to the fraction of power lost for a normal incident plane wave propagating across the surface.  $\alpha'_s$  is an important property of all surfaces in optics, yet it has historically rarely been measured[22], and is unknown today even for many important surfaces such as the *c*-Si surfaces studied here. From finite-element method (FEM) simulations[24], shown in Figure 1, the transverse magnetic (TM) polarization whispering-gallery-modes (WGMs) of the microdisk are  $\sim 90\times$  more sensitive to the top and bottom (100) Si surfaces than the etched sidewall at the microdisk periphery; specifically,  $\Gamma'_{top} = \Gamma'_{bot} = 3.5 \times 10^{-3} \text{ nm}^{-1}$  and  $\Gamma'_{side} = 8.1 \times 10^{-5} \text{ nm}^{-1}$ . This implies that  $\sim 0.2\%$  of the optical mode exists in a single monolayer at the top (bottom) Si surface, while little of the mode sees imperfections at the microdisk perimeter. At this level of sensitivity, a WGM with a  $Q = 1.5 \times 10^6$  (similar to the values measured in devices described below) can be used to measure fractional loss through the Si surface as small as  $\alpha'_s \sim 10^{-7}$ . Such high- $Q$  resonators can also be used to measure dispersive effects[25] of the Si surface chemistry with a sensitivity corresponding to 0.04% of a Si monolayer, or roughly  $\sim 10^4$  Si atoms for a  $5 \mu\text{m}$  radius microdisk.

The silicon microdisks studied in this work were fabricated from an SOI wafer commercially available from SOITEC, consisting of a 217 nm thick silicon device layer (*p*-type,  $14 - 20 \Omega\cdot\text{cm}$  resistivity,  $\langle 100 \rangle$  orientation) with a  $2 \mu\text{m}$   $\text{SiO}_2$  buried oxide (BOX) layer. Microdisks of 5 and  $10 \mu\text{m}$  radius were fabricated[26], finishing with a 10 minute acetone soak and Piranha etch to remove organic materials. A 1 hour dilute hydrofluoric acid (HF) solution comprised of five parts 18.3 MΩ deionized (DI) water to one part concentrated aqueous HF (49%) was used to remove a protective  $\text{SiN}_x$  cap and partially undercut the disk, as shown in the SEM micrograph in Figure 1(a).

The wafer was then rinsed in deionized water, dried with nitrogen ( $\text{N}_2$ ), and immediately transferred into an  $\text{N}_2$  purged testing enclosure.

The microdisk resonators were characterized using a tunable external-cavity laser ( $\lambda = 1420\text{-}1498$  nm, linewidth  $< 5$  MHz) connected to a computer-controlled fiber taper waveguide probe[27]. The micron-scale fiber taper probe was formed from a standard single-mode optical fiber and was used to evanescently excite the WGMs of the microdisk with controllable loading. Figure 2 shows the normalized spectral transmission response of a  $5 \mu\text{m}$  radius microdisk resonator, illustrating clear families of modes having similar linewidth,  $\delta\lambda$ , and free-spectral-range (FSR). By comparison to FEM simulations of the Si microdisk, each mode in Figure 2 was categorized and labelled as  $\text{TM}_{p,m}$ , where  $p$  and  $m$  are the radial and azimuthal number, respectively.

Owing to their large surface sensitivity (see Figure 1), the spectral signature of the  $\text{TM}_{1,m}$  modes was used to determine the quality of the optical surfaces. Figure 2(b) shows a high resolution scan across the  $\text{TM}_{1,31}$  mode. The observed double resonance dip, termed a doublet, is a result of surface roughness coupling of the normally degenerate clockwise (CW) and counter-clockwise (CCW) propagating WGMs[26, 28, 29]. The rate at which photons are back-scattered is quantified by the doublet splitting,  $\Delta\lambda$ , while the rate at which photons are lost from the resonator is quantified by the intrinsic linewidth,  $\delta\lambda$ , of the individual doublet modes. From a fit to the transmission spectrum of Fig. 2(b),  $\Delta\lambda = 11.9$  pm and  $\delta\lambda = 2.2$  pm, corresponding to an intrinsic modal quality factor of  $Q_i \equiv \lambda_0/\delta\lambda = 6.8 \times 10^5$  for this  $\text{TM}_{1,31}$  mode. This should be contrasted with the transmission spectrum shown in Fig. 2(c) for a more confined, and less surface sensitive, TE WGM of a much larger  $40 \mu\text{m}$  radius microdisk. From the fit parameters ( $\Delta\lambda = 0.8$  pm,  $\delta\lambda = 0.3$  pm), the  $Q$  of the buried TE mode is

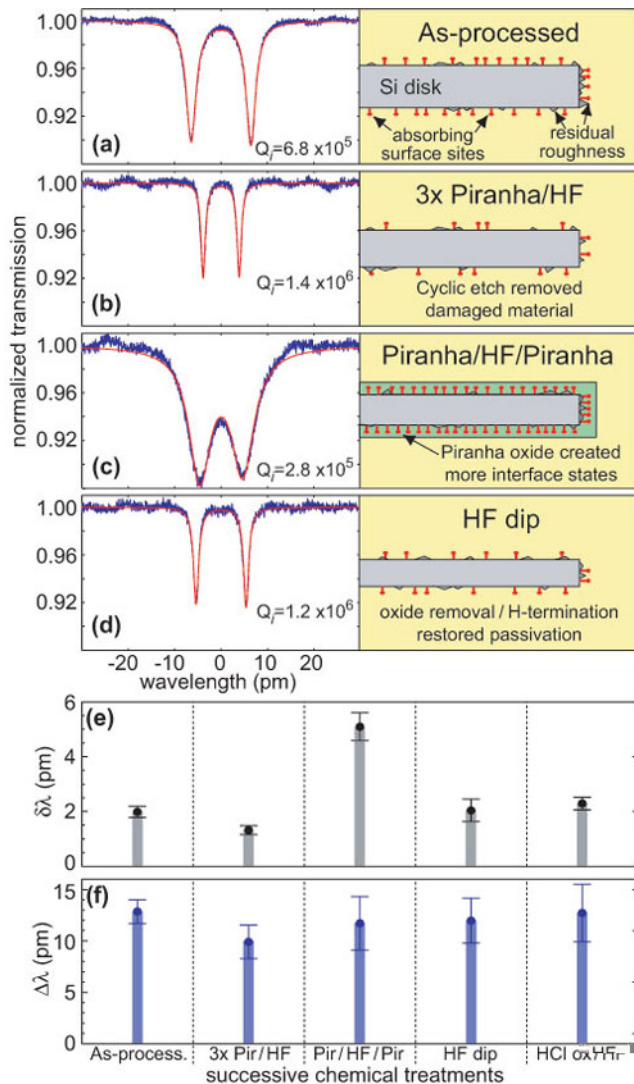


FIG. 3: (a-d) Taper transmission versus wavelength showing  $TM_{1,31}$  doublet mode after each chemical treatment and accompanying schematic of chemical treatment. (a) As-processed, (b) Triple Piranha/HF cycle described in Table I, (c) Single Piranha/HF cycle followed by an additional Piranha step allowing controlled measurement of piranha oxide, and (d) HF dip to remove chemical oxide from previous treatment and restore passivation. (e) Average intrinsic linewidth,  $\delta\lambda$  and (f) average doublet splitting,  $\Delta\lambda$ , for all  $TM_{1,m}$  modes within the 1420-1470 nm spectrum after each chemical treatment step.

$Q_i = 4.7 \times 10^6$ , corresponding to a loss per unit length of  $\alpha_i = 0.13$  dB/cm. This is nearly an order of magnitude smaller optical loss than that of the as-processed  $TM_{1,m}$  modes, and provides an upper bound on the bulk Si optical loss of the SOI material.

The stark difference between the surface-sensitive TM and bulk TE modes indicates that the as-processed Si surfaces are far from optimal. Etch-induced surface damage on the microdisk sidewall can only account for a small fraction of this difference due to the enhanced sensitivity

of the  $TM_{1,m}$  to the top and bottom Si surfaces (comparison of the TM and TE modes in the same microdisk and with similar modal overlap with the microdisk edge bear this out). Damage to the top and bottom Si surfaces can stem from a variety of possible sources including chemical mechanical polishing, native oxide formation during storage, or adventitious organic matter[3]. In an attempt to repair the Si surfaces a series of chemical oxidation treatments were performed on the devices. The well-known process [2, 6, 30] of repeated chemical oxidation in Piranha ( $H_2SO_4/H_2O_2$ ) and HF oxide stripping was employed to controllably prepare the Si surfaces. Three cycles of the Piranha/HF process, recipe shown in Table I, were applied to the as-processed devices. From the blue-shift in the WGM resonances due to the three cycles of the Piranha/HF process, an estimated  $1.9 \pm 0.1$  nm of Si was removed from the surface of the microdisk. The fit to the  $TM_{1,31}$  transmission spectrum, shown in Figure 3(b), indicates that a significant improvement to the surfaces has also taken place, yielding a  $\Delta\lambda = 9.7$  pm and  $\delta\lambda = 1.1$  pm.

To separate the effects of the Piranha oxidation and the HF etch, the sample was put through a Piranha/HF/Piranha treatment. The first cycle of Piranha/HF was used to “refresh” the hydrogen passivation before re-oxidizing the Si surface with Piranha. Figure 3(c) shows the fit to the now barely resolvable  $TM_{1,31}$  doublet yielding  $\Delta\lambda = 8.6$  pm and  $\delta\lambda = 5.6$  pm. The five-fold increase in linewidth and a negligible increase in doublet splitting is indicative of a significant activation of absorbing surface states without an increase in surface scattering. Removing the chemical oxide with the HF dip listed in Table I and retesting indicated that an oxide film equivalent to  $2.8 \pm 0.1$  nm of  $SiO_2$  had been present. The fit to the transmission spectrum of the  $TM_{1,31}$  mode in Figure 3(d) yielded fit parameters  $\Delta\lambda = 9.7$  pm and  $\delta\lambda = 1.2$  pm, showing that the optical damage to the Si surfaces caused by Piranha oxidation was reversible.

As a final treatment to the  $5 \mu m$  radii microdisks, we used the same  $3 \times$  oxidation and stripping process as described in Table I, but with an HCl based chemistry ( $8:1:2 H_2O:HCl:H_2O_2$ , heated to  $60^\circ C$ ) instead of the  $H_2SO_4$  based chemistry. Figure 3(e-f) shows a graphical representation of the average behavior of all  $TM_{1,m}$  modes in the 1420-1470 nm span after each chemical treatment. The results reveal that the HCl oxidation was slightly less effective at passivating the silicon surface than the Piranha oxidation; however, it is expected that the optimum solution for chemical oxidation will depend upon the Si crystal orientation and previous chemical treatments[5, 8].

Although it has recently been observed[30] that repeated chemical oxidation and removal of silicon can provide a smoothing action on etched sidewalls, the large shifts in optical loss with chemical treatment described above can be linked to surface-state absorption as opposed to surface-scattering. Whereas the highly confined Si waveguide measurements to date have been sensitive

TABLE I: Summary of successive steps for a piranha oxidation surface treatment

Step	Composition <sup>a</sup>	Temp.	Time
Piranha	3:1 H <sub>2</sub> SO <sub>4</sub> /H <sub>2</sub> O <sub>2</sub>	100°C	10 min
Rinse	DI H <sub>2</sub> O	23°C	30 sec
Rinse	DI H <sub>2</sub> O	23°C	30 sec
Rinse	DI H <sub>2</sub> O	23°C	30 sec
HF dip	10:1 H <sub>2</sub> O/HF	23°C	1 min
Rinse	DI H <sub>2</sub> O	23°C	15 sec
Rinse	DI H <sub>2</sub> O	23°C	15 sec

<sup>a</sup>All ratios are quoted by volume of standard concentration aqueous solutions

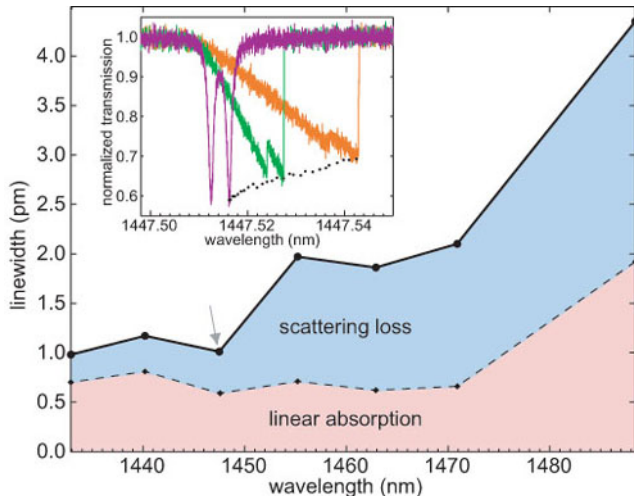


FIG. 4: Wavelength dependent intrinsic linewidth for a 10  $\mu\text{m}$  radius microdisk. Also shown is the delineation between scattering loss versus linear absorption after six cycles of the Piranha/HF treatment given in Table I. (inset) Examples of the power dependent transmission versus wavelength data used to separate the absorption from the total loss for the  $\text{TM}_{1,m}$  mode at  $\lambda = 1447.5$  nm.

to changes in loss as low as 1 dB/cm, the microdisks of this work are sensitive to changes of loss more than an order of magnitude smaller ( $< 0.03$  dB/cm) where surface chemistry is more likely to play a role. Indeed, as mentioned above the TM-polarized microdisk WGMs are selectively sensitive to the top and bottom Si surfaces which are extremely smooth in comparison to etched surfaces. The negligible change in average mode-splitting,  $\Delta\lambda$ , with chemical treatment (Figure 3(f)) is also indicative of little change in surface roughness.

In order to confirm the above assumption, and to measure the efficacy of the surface-state passivation of the Piranha/HF chemistry, the wavelength dependent optical quality was measured on 10  $\mu\text{m}$  radii disks subjected to a  $6\times$  Piranha/HF treatment. FEM simulations show that 10  $\mu\text{m}$  radii disk have approximately the same fractional energy overlap with the top/bottom Si surfaces ( $\Gamma'_{top} = \Gamma'_{bot} = 3.7 \times 10^{-3} \text{ nm}^{-1}$ ) as 5  $\mu\text{m}$  radii disks but have roughly half the fractional energy overlap with the etched sidewalls ( $\Gamma'_{side} = 3.8 \times 10^{-5} \text{ nm}^{-1}$ ). Figure 4

shows a plot of the wavelength dependent loss across the full 1420 – 1500 nm span for the  $\text{TM}_{1,m}$  modes of a 10  $\mu\text{m}$  radius disk, showing a strong trend towards increasing optical loss with wavelength. The black line indicates the intrinsic linewidth for each  $m$  number, with an error bar of  $\pm 0.05$  pm per point (not shown). The separation of scattering loss and linear absorption was obtained using a modified version of the power dependent measurements described in Reference [26]. This technique uses the local temperature increase of the silicon microdisk to determine the absorption component of loss, similar to PDS, but without the need for a thermal model for heat flow; rather, the onset of two-photon absorption changes the fraction of absorption as a function of power, allowing the linear absorption coefficient to be ascertained directly. The inset to Fig. 4 shows three examples of power dependent transmission spectra for the 1447.5 nm mode (grey arrow), along with corresponding transmission minima versus wavelength (black dots).

From the optical loss measurements of Fig. 4 it is clear that a significant fraction of residual optical loss, after Piranha/HF treatment and hydrogen surface passivation, is still due to surface-state absorption (bulk absorption is negligible at this level). The strong trend of increasing optical loss with wavelength is seen to be dominated by elastic scattering and/or radiation loss, with the surface-state absorption being relatively constant across the  $\lambda = 1420$ -1500 nm spectrum. Through measurements of the radiation limited quality factors of  $\text{TM}_{1,m}$  modes in the longer wavelength 1565-1625 nm band, intrinsic radiation losses from the circular microdisk are found to contribute negligibly to the losses in Fig. 4. FEM simulations also show that  $\Gamma'$  on all of the surfaces changed less than 5% over the  $\lambda = 1420$ -1500 nm span. The most likely explanation for the observed wavelength dependant loss is improved phase-matching of surface-scattering into radiation modes with increasing wavelength.

By comparing the cavity  $Q$  before and after the Piranha oxide removal, a fractional surface absorption loss per pass of  $\alpha'_{s,ox} \sim 2 \times 10^{-5}$  is estimated for the Piranha oxide. This large fractional absorption in the  $\lambda = 1400$  nm wavelength band ( $\hbar\omega \sim 0.85$  eV) is attributed to single-photon absorption by mid-gap interface states. Such electronic interface states at the Si/(Piranha)SiO<sub>x</sub> interface have been observed in Ref. [4], with three sets of state-density maxima in the bandgap of silicon occurring at 0.3, 0.5, and 0.7 eV above the valence-band maximum. In comparison, from Figure 4, the modal absorption loss of the hydrogen-passivated Si surface is as small as  $\alpha'_m \sim 0.08 \text{ cm}^{-1}$ , corresponding to a fractional surface absorption loss per pass of  $\alpha'_{s,H} \sim 2 \times 10^{-6}$  for the top (bottom) Si active layer surface.

All of the measurements described above were performed in a N<sub>2</sub> purged environment over several weeks. Even in such an environment, however, changes in the hydrogen passivated surfaces were observed over times as short as a few days. Left in an unprotected air environment, degradation of the optical surface quality was

evident in a matter of hours. Research and development of stable surface passivation techniques optimized for optical quality, akin to the gate oxides of CMOS microelectronics, will be a key ingredient in the future development of Si photonics. Our data suggests that surface chemistry as much as surface roughness will ultimately

limit the performance of Si microphotonic devices, and further development of Si passivation techniques should be able to reduce optical losses by as much as an order of magnitude (towards the bulk  $c$ -Si limit) while simultaneously improving the stability and manufacturability of future Si photonic components.

- 
- [1] Yablonovitch, E., Allara, D. L., Chang, C. C., Gmitter, T. & Bright, T. B. Unusually low surface-recombination velocity on silicon and germanium surfaces. *Phys. Rev. Lett.* **57**, 249–252 (1986).
- [2] Chabal, Y., Higashi, G. & Raghavachari, K. Infrared spectroscopy of si(111) and si(100) surfaces after hf treatment: Hydrogen termination and surface morphology. *J. Vac. S. Tech. A* **7**, 2104–2109 (1989).
- [3] Fenner, D., Biegelsen, D. & Bringans, R. Silicon surface passivation by hydrogen termination: A comparative study of preparation methods. *J. Appl. Phys.* **66**, 419–424 (1989).
- [4] Yamashita, Y., Asano, A., Nishioka, Y. & Kobayashi, H. Dependence of interface states in the si band gap on oxide atomic density and interfacial roughness. *Phys. Rev. B* **59**, 872–881 (1999).
- [5] Kobayashi, H., Yamashita, Y., Nakato, Y., Komeda, T. & Nishioka, Y. Interface states at ultrathin oxide/si(111) interfaces obtained from x-ray photoelectron spectroscopy measurements under biases. *Appl. Phys. Lett.* **69**, 2276–2278 (1996).
- [6] Linnros, J. Carrier lifetime measurements using free carrier absorption transients. ii. lifetime mapping and effects of surface recombination. *J. Appl. Phys.* **84**, 284–291 (1998).
- [7] Li, F., Balazs, M. K. & Anderson, S. Effects of ambient and dissolved oxygen concentration in ultrapure water on initial growth of native oxide on a silicon (100) surface. *J. Electrochem. Soc.* **152**, G669–G673 (2005).
- [8] Petitdidier, S. *et al.* Growth mechanism and characterization of chemical oxide films produced in peroxide mixtures on si(100) surfaces. *Thin Solid Films* **476**, 51–58 (2005).
- [9] Muller, D. A. A sound barrier for silicon? *Nature Materials* **4**, 645–647 (2005).
- [10] Liu, A. *et al.* A high-speed silicon optical modulator based on a metal-oxide-semiconductor capacitor. *Nature* **427**, 615–618 (2004).
- [11] Xu, Q., Schmidt, B., Pradhan, S. & Lipson, M. Micrometre-scale silicon electro-optic modulator. *Nature* **435**, 325–327 (2005).
- [12] Boyraz, O. & Jalali, B. Demonstration of a silicon raman laser. *Opt. Express* **12**, 5269–5273 (2004).
- [13] Rong, H. *et al.* A continuous-wave raman silicon laser. *Nature* **433**, 725–728 (2005).
- [14] Notomi, M. *et al.* Optical bistable switching action of Si high- $Q$  photonic-crystal nanocavities. *Opt. Express* **13**, 2678–2687 (2005).
- [15] Tanabe, T., Notomi, M., Mitsugi, S., Shinya, A. & Kuramochi, E. Fast bistable all-optical switch and memory on a silicon photonic crystal on-chip. *Opt. Lett.* **30**, 2575–2577 (2005).
- [16] Song, B., Noda, S., Asano, T. & Akahane, Y. Ultra-high- $q$  photonic double-heterostructure nanocavity. *Nature Materials* **4**, 207–210 (2005).
- [17] Vahala, K. J. Optical microcavities. *Nature* **424**, 839–846 (2003).
- [18] Lang, D. V. Deep-level transient spectroscopy: A new method to characterize traps in semiconductors. *J. Appl. Phys.* **45**, 3023–3032 (1974).
- [19] Chantre, A., Vincent, G. & Bois, D. Deep-level optical spectroscopy in gaas. *Phys. Rev. B* **23**, 5335–5358 (1981).
- [20] Aarts, I. M. P. *et al.* Direct and highly sensitive measurement of defect-related absorption in amorphous silicon thin films by cavity ringdown spectroscopy. *Appl. Phys. Lett.* **84**, 3079–3081.
- [21] Jackson, W. B. & Amer, N. M. Direct measurement of gap-state absorption in hydrogenated amorphous silicon by photothermal deflection spectroscopy. *Phys. Rev. B* **25**, 5559–5562 (1982).
- [22] Amato, G. & Fizzotti, F. Gap-states distribution in amorphous-silicon films as obtained by photothermal deflection spectroscopy. *Phys. Rev. B* **45**, 14108–14113 (1992).
- [23] Blood, P. On the dimensionality of optical absorption, gain, and recombination in quantum-confined structures. *IEEE J. Quan. Elec.* **36**, 354–362 (2000).
- [24] Spillane, S. M. *et al.* Ultrahigh- $q$  toroidal microresonators for cavity quantum electrodynamics. *Phys. Rev. A* **71**, 013817 (2005).
- [25] Teraoka, I., Arnold, S. & Vollmer, F. Perturbation approach to resonance shifts of whispering-gallery modes in a dielectric microsphere as a probe of a surrounding medium. *J. Opt. Soc. Am. B* **20**, 1937–1946 (2003).
- [26] Borselli, M., Johnson, T. J. & Painter, O. Beyond the rayleigh scattering limit in high- $q$  silicon microdisks: theory and experiment. *Opt. Express* **13**, 1515–1530 (2005).
- [27] Borselli, M., Srinivasan, K., Barclay, P. E. & Painter, O. Rayleigh scattering, mode coupling, and optical loss in silicon microdisks. *Appl. Phys. Lett.* **85**, 3693–3695 (2004).
- [28] Gorodetsky, M., Pryamikov, A. & Ilchenko, V. Rayleigh scattering in high- $q$  microspheres. *J. Opt. Soc. Am. B* **17**, 1051–1057 (2000).
- [29] Little, B. E., Laine, J.-P. & Chu, S. T. Surface-roughness-induced contradirectional coupling in ring and disk resonators. *Opt. Lett.* **22**, 4–6 (1997).
- [30] Sparacin, D. K., Spector, S. J. & Kimerling, L. C. Silicon waveguide sidewall smoothing by wet chemical oxidation. *J. Lightwave Tech.* **23**, 2455–2461 (2005).